Microwave technique for detection, location and sizing of buried objects

Latifa Achrait-Furlan, T. Lasri, Ahmed Mamouni

MICROWAVE TECHNIQUE FOR DETECTION, LOCATION, AND SIZING OF BURIED OBJECTS

L. Achrait-Furlan,[1] T. Lasri,[1] and A. Mamouni[1]
[1] Institut d'Electronique et de Microélectronique du Nord
UMR CNRS 8520
IEMN – DHS
59652 Villeneuve d'Ascq Cedex, France

ABSTRACT: *The detection, location, and sizing of immersed objects in a host medium are tasks of interest in many fields. One of the most suitable tools for the noninvasive measurements of buried objects is the use of microwaves. We propose in this paper a microwave method based on the knowledge of the reflection coefficient.*

Key words: *microwaves; noninvasive; reflection coefficient; heterogeneous medium; buried objects*

I. INTRODUCTION

The detection and/or identification of buried objects [1–3] is a very important problem for environmental, military, and humanitarian purposes. Several fields, such as geophysics, civil engineering, medicine, or the food industry, are concerned.

The techniques principally employed are based on the use of ground-penetrating radars (GPRs) which are now commonly used in many applications (mines, cables, or pipe detection). Nevertheless, for the detection of small objects at shallow depth, this method is not as efficient as expected. For these kinds of studies, we propose an alternative method based on the measurement of the reflection coefficient of the medium under test. In particular, modeling studies have been performed in order to predict the reflection coefficient of different structures. These theoretical results have been compared to experimental ones, obtained with an *S*-parameter measurement system (SPMS-2450) developed in the laboratory [4]. Examples are used to illustrate the method to determine the location and dimensions of a buried object.

II. SIMULATION AND MEASUREMENT METHODS

In order to detect nonmetallic mines or to localize cables, pipes, or parasitic inclusions in a host medium, ground-penetrating radars (GPRs) are generally used.

We present here a complementary method based on the measurement of the reflection coefficient at 2.45 GHz [5–7]. The test setup presented in Figure 1 consists of a PVC tank, $150 \times 150 \times 150$ mm^3, where the inclusion to be characterized is inserted. Three rectangular apertures have been made on three walls of the box, so that the microwave signal is applied to the test structure through a probe. The probes (P_i) are rectangular waveguides filled with a low-loss dielectric material. The experiments have been performed using inclusions which are hollow plastic pieces that can be filled with various dielectric materials. The measurement of the reflection coefficient $S_{11} = |S_{11}|e^{j\varphi_{S_{11}}}$ of the device under test is made by using a system, operating at 2.45 GHz, developed in the laboratory, called the *S*-parameter measurement system (SPMS-2450).

Two different methods are used to predict the reflection coefficient. The first one, called the modal method [8] and based on the continuity of the propagation modes between the waveguide and a dissipative medium, is well suited to study homogeneous or multilayer materials. In the case of more complicated structures, such as inclusions in a host medium, we make use of the three-dimensional electromagnetic simulation software, Ansoft's High Frequency Structure Simulator (HFSS).

III. RESULTS

A. Estimation of the Inclusion Cross Section. In this work, the inclusions considered are cubic or cylindrical plastic-made hollow pieces filled with glycerol or water, whose permittivities at 2.45 GHz are, respectively, $\varepsilon_g^* = 5 - j0.8$ and $\varepsilon_w^* = 77 - j12$. The host medium is sand ($\varepsilon_s^* = 3.2 - j0.05$ at 2.45 GHz).

The cubic pieces have either a 33 or 40 mm side, while the cylindrical pieces considered are such that: diameter = height = either 33 or 40 mm.

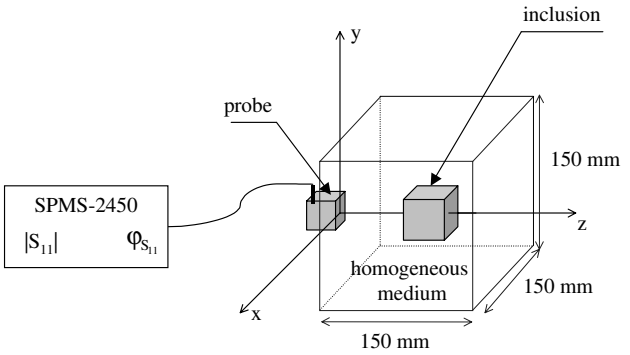

Figure 1 Schematic description of the test setup ($F = 2.45$ GHz)

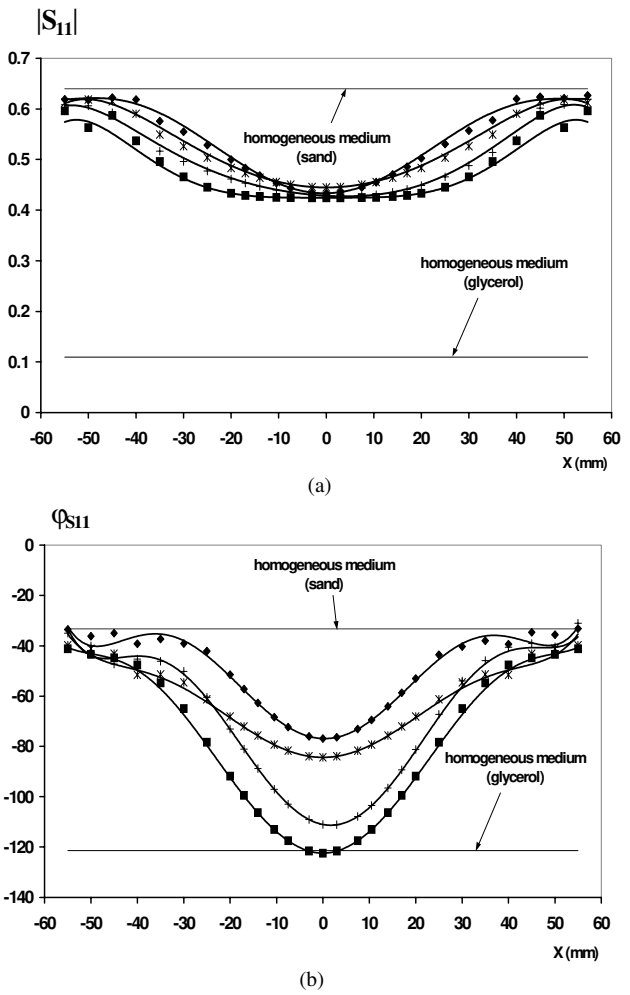

Figure 2 Reflection coefficient simulated by means of HFSS versus the lateral position (x) of the inclusion filled with glycerol, immersed in sand, and located at the surface ($z = 0$). Probe used: P_1, $F = 2.45$ GHz. (a) Magnitude of S_{11}. (b) Phase of S_{11}. ■: cube (side 40 mm), *: cube (side 33 mm), +: cylinder (diameter = height = 40 mm), ♦: cylinder (diameter = height = 33 mm)

The results presented hereafter (Fig. 2) are obtained using the probe P_1 (waveguide 58×28 mm^2 filled with a low-loss material whose permittivity is $\varepsilon_d = 4$). The operating frequency is 2.45 GHz. The structure is scanned along the Ox-axis (Fig. 1), and for each position, the reflection coefficient is recorded. The height of the cylinder is along the propagation axis Oz, and the circular cross section is parallel to the cross section of the waveguide. In these graphs, we have also reported the results obtained when the tank is only filled with a homogeneous (without inclusion) medium (sand or glycerol).

We note that the presence of the inclusion is clearly observed. Moreover, the influence of the geometrical shapes and sizes is also evidenced. However, even if the differentiation between two geometrical shapes of the same size is difficult, it appears that both the magnitude and phase of S_{11} depend on the geometrical shape of the piece under investigation.

Due to the size of the tested inclusions compared to the aperture of the waveguide probe (58×28 mm^2), the magnitude of the reflection coefficient at $x = 0$ is very far from the one obtained when only glycerol is present (homogeneous medium). In this case, it is very difficult to use the magnitude of the reflection coefficient $|S_{11}(x)|$ to distinguish the shape and size of the inclusions.

The same experiments are made with the inclusion located at $z = 5$ mm from the interface waveguide–host dissipative medium (Fig. 3). The conclusions drawn from the responses recorded are very close to those stated for $z = 0$ mm. In particular, these results point out that the subsurface location and sizing are conceivable.

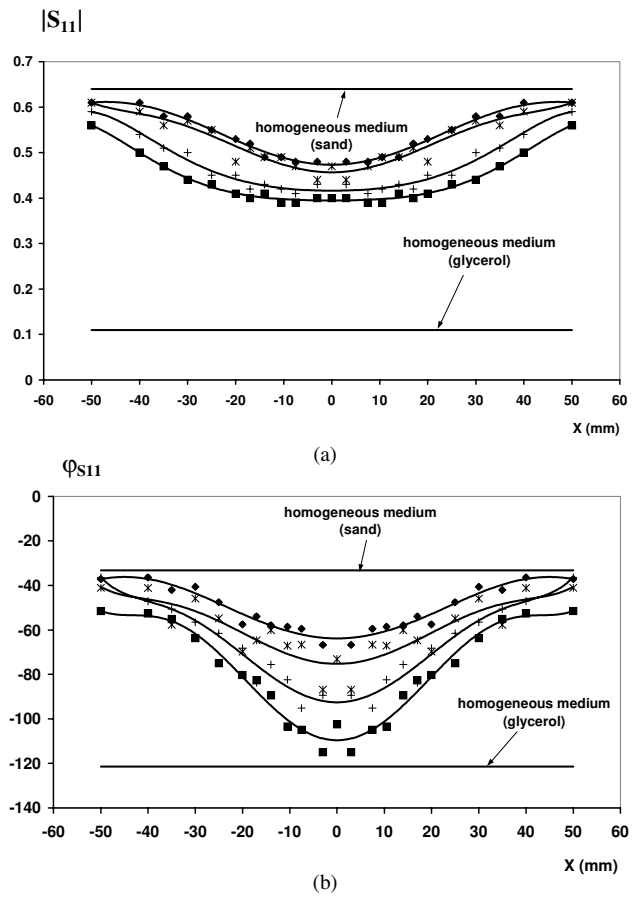

Figure 3 Reflection coefficient simulated by means of HFSS versus the lateral position (x) of the inclusion filled with glycerol, immersed in sand, and located at $z = 5$ mm. Probe used: P_1, $F = 2.45$ GHz. (a) Magnitude of S_{11}. (b) Phase of S_{11}. ■: cube (side: 40 mm), *: cube (side: 33 mm), +: cylinder (diameter = height = 40 mm), ♦: cylinder (diameter = height = 33 mm)

TABLE 1 Determination of the Inclusion Cross Section

Inclusion		Cube (mm) (Side = 40 mm)	Cylinder (mm) ($d = h = 40$ mm)	Cube (mm) (Side = 33 mm)	Cylinder (mm) ($d = h = 33$ mm)
$Z = 0$ mm	Dimension measured using $\lvert S_{11}\rvert$	62	54	43	35
	Dimension measured using $\varphi_{S_{11}}$	36	32.5	38	27
$Z = 5$ mm	Dimension measured using $\lvert S_{11}\rvert$	60	48	34	34
	Dimension measured using $\varphi_{S_{11}}$	28	34	34	34

Before reporting the results of the estimated cross section of the different tested inclusions, we present the method used to determine these sections.

One can note that the shape of the plots presented in Figures 2 and 3 appears like a Gaussian form. Thus, by means of a currently used method, which consists of measuring the -3 dB width in order to characterize the width of the radiation pattern of an antenna, it is possible to obtain an estimation of the dimensions of the object under test.

It can also be seen that the width of the $S_{11}(x)$ curves depends on the dimensions of the inclusions: the width gets larger as the dimensions of the inclusion increase. Therefore, the measurement of the width of the curves (both in magnitude and phase) can lead to an approximation of the inclusion cross section (Table 1).

These results show that it is possible to evaluate the width of the inclusion. However, it can be noted that the accuracy of this determination depends on the shape of the tested object and on the parameter used (magnitude or phase). When small objects are to be detected, we obtain a better result when phase values of S_{11} are used. The mean value for the error on the cross-section estimation is about 15% when the phase is used instead of about 25% when the magnitude is considered.

As a conclusion, we have shown that it is possible to locate the inclusion (along the *Ox*-axis) and estimate its cross section in a host medium through the determination of the reflection coefficient.

B. Influence of the Inclusion Location in Depth. In the previous section, it was demonstrated that the location of an inclusion along the scanning axis can be achieved. In this paragraph, we propose to describe the influence of the inclusion depth on the location possibilities.

When the cross section of the inclusion is very large compared to the waveguide aperture, one can approximate the structure to be tested to a three-layer one. The modal method can then be applied, and allows us to have a quick answer about the dependence of the reflection coefficient versus the layered structure.

Figure 4 gives the results obtained when a three-layer medium and a structure which is made of an inclusion buried in a homogeneous environment are considered. The materials selected for these tests are sand (host medium) and water (inclusion).

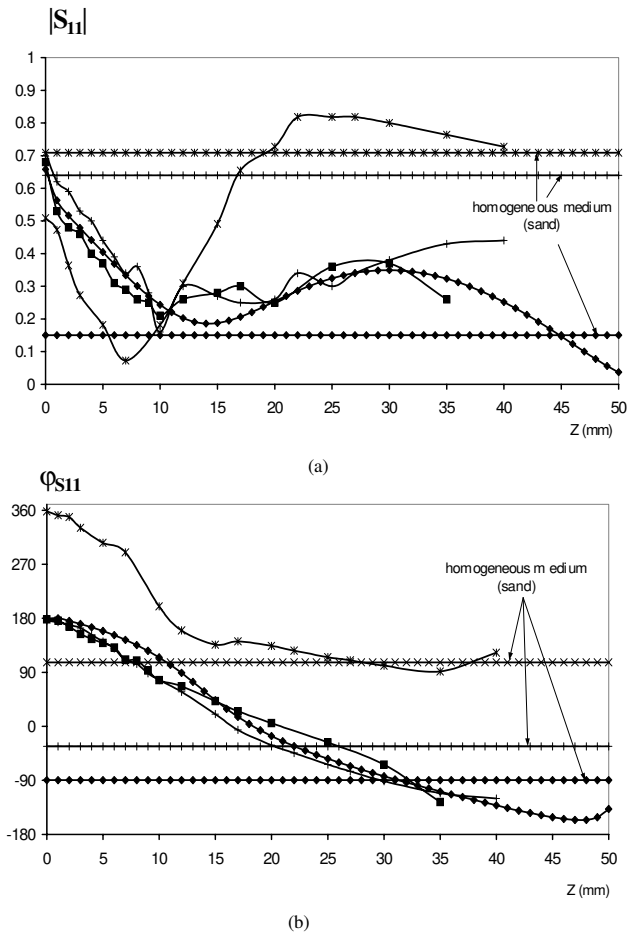

Figure 4 Reflection coefficient versus the longitudinal position (z) of the cubic inclusion (side: 40 mm) filled with water, immersed in sand, and located at $x = 0$ mm. Probe used: P_1, $F = 2.45$ GHz. (a) Magnitude of S_{11}. (b) Phase of S_{11}. *: measurements (SPMS-2450), ♦: modal method, ■: HFSS (three layers), +: HFSS (host medium + inclusion)

Three kinds of simulation data have been used to plot these graphs. The software HFSS provides the responses for the two cases proposed, while the modal method deals only with the three-layer medium. The fourth curve given in this figure corresponds to the reflection coefficient measurement, by means of the SPMS-2450, of the host medium–inclusion

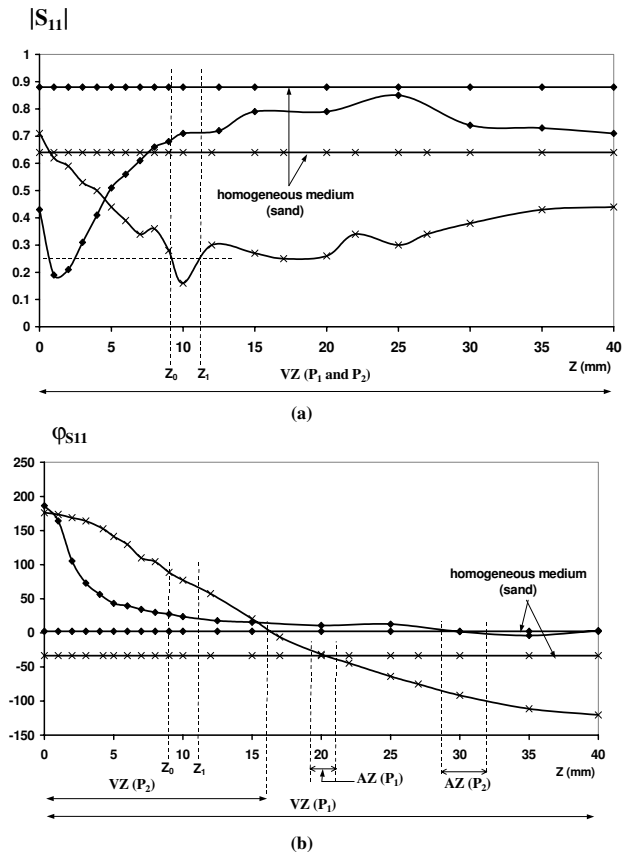

Figure 5 Reflection coefficient simulated by means of HFSS versus the longitudinal position (z) of the cubic inclusion (side: 40 mm) filled with water, immersed in sand, and located at $x = 0$ mm, $F = 2.45$ GHz. (a) Magnitude of S_{11}. (b) Phase of S_{11}. *: P_1, ♦: P_2

structure. Measurements of a three-layer medium have not been conducted in this study.

Despite the aperture of the probe being larger than the cross section of the inclusion under test, we note that the heterogeneous structure can be approximated to a three-layer model. The HFSS simulation results for the host medium–inclusion structure and for the three-layer material are roughly the same. The shapes of the variations of the measured (SPMS-2450) and simulated (modal method and HFSS method) reflection coefficient versus z agree for depths below 15 mm. Another reason that explains the discrepancies between the measured and computed data is related to the dimension of the tank. These have been initially chosen so that the edge effects can be neglected at 2.45 GHz when the homogeneous material that fills the box is water or glycerol. In the case of sand, the dimensions required to fulfill this condition are larger than the actual ones. We have not rebuilt a box especially for this material, knowing that, in most cases, we have to deal with moist sand for which smaller dimensions are needed. The aim of this experiment is just to have an idea of the behavior of the reflection coefficient when testing this kind of material. Many kinds of inclusions with various shapes and sizes have been tested by this method [6, 7].

We present in Figure 5 the simulation results obtained when two different probes are considered. On this graph, two zones have been defined: a visibility zone (VZ) corresponding to the z-value from which the reflection coefficient tends toward the host medium's one, and an ambiguity zone (AZ) related to a zone where there is some doubt about the presence (or absence) of an inclusion.

One can observe that, when the magnitude of S_{11} is considered, the inclusion is always seen, using either P_1 or P_2 (waveguide 28×14 mm^2 filled with a low-loss material whose permittivity is $\varepsilon_d = 16$). The presence of an AZ for probe P_1 is noted.

If the phase of S_{11} is used, it can be seen that P_2 allows us to have a VZ around 16 mm. For P_1, a VZ up to 40 mm is obtained, and the presence of an AZ is seen around 20 mm.

An important issue that is also emphasized here is the ambiguity that can arise when a location, in depth, is aimed. A solution to overcome this problem is to use several probes. To illustrate the method to remove the uncertainty of the inclusion position, we refer to Figure 5. Due to the non-monotonous shape of the magnitude of the reflection coefficient, for a magnitude value, we may have two possible depths (Z_0 and Z_1). To choose between these two candidates, we make use of the results given by another probe (here, P_2).

The knowledge of the phase of the reflection coefficient sometimes may be sufficient to solve this problem without having recourse to a measurement with another probe (Fig. 5). In fact, the use of several probes lowers the risk of indetermination. It is a way to compensate, a bit, for the fact that we operate only at one frequency.

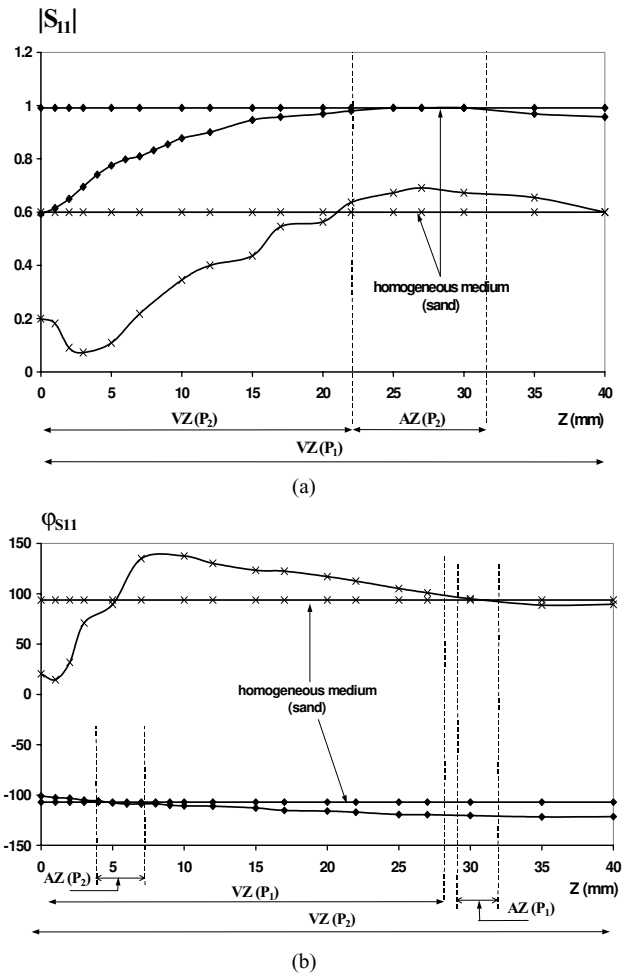

Figure 6 Reflection coefficient simulated by means of HFSS versus the longitudinal position (z) of the cubic inclusion (side: 40 mm) filled with glycerol, immersed in sand, and located at $x = 0$ mm, $F = 2.45$ GHz. (a) Magnitude of S_{11}. (b) Phase of S_{11}. *: P_1, ♦: P_2

The same kind of test has been made in the case of an inclusion filled with glycerol. The measurement results given in Figure 6 lead to similar conclusions.

IV. CONCLUSION

This paper shows the ability to detect an object in a host medium and to obtain an estimation of its cross section, using a noninvasive microwave technique which consists of the reflection coefficient measurement.

The dielectric inclusions tested are filled with low- or high-loss dielectric materials, which allow us to obtain low- or high-permittivity contrasts between the host medium (sand) and the dielectric inclusion. In both cases, we obtain acceptable visibility zones, and the cross section of the object is estimated with an accuracy of about 20% in most cases.

The accuracy of the measurements can be increased by using probes with different sizes and dielectric characteristics. This method is a complementary one to the GPR method.

REFERENCES

1. C. Rappaport and E. Miller, Physics-based modeling and inverse scattering for detection of buried mine-shape anomalies, SPIE, Denver, CO, July 1999, vol. 3752, pp. 274–284.
2. D.J. Daniels, Advances in the ultrawideband radar imaging of buried mines, Progr Electromag Res Symp (PIERS), Nantes, France, July 1998, vol. 2, p. 860.
3. J. Cashman, C. Pichot, and J.-Y. Dauvignac, Imaging of buried objects from multi-look, multifrequency radar data in the Fourier domain, including antenna effects, Progr Electromag Res Symp (PIERS), Nantes, France, July 1998, vol. 2, p. 863.
4. T. Lasri, D. Glay, A. Mamouni, and Y. Leroy, Development of microwave moisture measurement systems around microstrip complex correlators, Sensors update, Wiley–VCH Verlag GmbH, Germany, 2000, vol. 7, chap. 9, pp. 233–248.
5. T. Lasri, D. Glay, L. Achraït, A. Mamouni, and Y. Leroy, Microwave methods and systems for nondestructive control, Subsurface Sensing Technol Appl, Int J 1 (2000), pp. 141–160.
6. L. Achraït, T. Lasri, and A. Mamouni, Détection d'objets enterrés par des techniques microondes, JCMM'2000, Paris, France, Mar. 2000.
7. L. Achraït, T. Lasri, and A. Mamouni, Simulation et mesure du coefficient de réflexion de structures hétérogènes, 12th J Nat Microondes, Poitiers, France, May 2001.
8. T. Lasri, K. Ridaoui, B. Bocquet, A. Mamouni, and Y. Leroy, Absolute weighting functions for near-field microwave radiometric applications, J Electromag Waves Appl 13 (1999), 1237–1365.